Design and fabrication of a hybrid alginate hydrogel/poly(ε-caprolactone) mold for auricular cartilage reconstruction

D. O. Visscher,[1] **A. Gleadall**,[2,3] **J. K. Buskermolen**,[4] **F. Burla**,[5] **J. Segal**,[2] **G. H. Koenderink**,[5] **M. N. Helder**,[6] **P. P. M. van Zuijlen**[1,7,8]

[1]Department of Plastic, Reconstructive and Hand Surgery, Amsterdam University Medical Center, Amsterdam Movement Sciences, Amsterdam, The Netherlands
[2]Manufacturing and Process Technologies, Faculty of Engineering, University of Nottingham, Nottingham, England, UK
[3]Wolfson School of Mechanical and Manufacturing Engineering, Loughborough University, Leicestershire, LE11 3TU, UK
[4]Department of Dermatology, Amsterdam University Medical Center, Amsterdam Movement Sciences, Amsterdam, The Netherlands
[5]Department of Living Matter, AMOLF, Amsterdam, The Netherlands
[6]Department of Oral and Maxillofacial Surgery/Oral Pathology, Amsterdam University Medical Center, Amsterdam Movement Sciences, Amsterdam, The Netherlands
[7]Department of Plastic, Reconstructive and Hand Surgery, Red Cross Hospital, Beverwijk, The Netherlands
[8]Association of Dutch Burn Centers, Beverwijk, The Netherlands

Received 5 April 2018; revised 14 August 2018; accepted 23 September 2018
Published online 00 Month 2018 in Wiley Online Library (wileyonlinelibrary.com). DOI: 10.1002/jbm.b.34264

Abstract: The aim of this study was to design and manufacture an easily assembled cartilage implant model for auricular reconstruction. First, the printing accuracy and mechanical properties of 3D-printed poly-ε-caprolactone (PCL) scaffolds with varying porosities were determined to assess overall material properties. Next, the applicability of alginate as cell carrier for the cartilage implant model was determined. Using the optimal outcomes of both experiments (in terms of (bio)mechanical properties, cell survival, neocartilage formation, and printing accuracy), a hybrid auricular implant model was developed. PCL scaffolds with 600 μm distances between strands exhibited the best mechanical properties and most optimal printing quality for further exploration. In alginate, chondrocytes displayed high cell survival (~83% after 21 days) and produced cartilage-like matrix in vitro. Alginate beads cultured in proliferation medium exhibited slightly higher compressive moduli (6 kPa) compared to beads cultured in chondrogenic medium (3.5 kPa, $p > .05$). The final auricular mold could be printed with 300 μm pores and high fidelity, and the injected chondrocytes survived the culture period of 21 days. The presented hybrid auricular mold appears to be an adequate model for cartilage tissue engineering and may provide a novel approach to auricular cartilage regeneration for facial reconstruction. © 2018 The Authors Journal of Biomedical Materials Research Part B: Applied Biomaterials published by Wiley Periodicals, Inc. J Biomed Mater Res B Part B: 00B: 000–000, 2018.

Key Words: cartilage, biopolymer, tissue scaffold, 3D printing, polycaprolactone, tissue engineering

How to cite this article: Visscher DO, Gleadall A, Buskermolen JK, Burla F, Segal J, Koenderink GH, Helder MN, van Zuijlen PPM. 2018. Design and fabrication of a hybrid alginate hydrogel/poly(ε-caprolactone) mold for auricular cartilage reconstruction. J Biomed Mater Res B Part B 2018:00:00:1–11.

INTRODUCTION

Auricular reconstruction following trauma (e.g., burns), cancer, or congenital anomalies is a very challenging procedure. To date, several treatment options exist to reconstruct a deformed auricle including synthetic implants (e.g., Medpor)[1–3] and autologous reconstruction using rib cartilage.[4–6] However, both techniques have several limitations including donor site morbidity,[7,8] risk of implant exposure,[1,9] and surgical complexity.[10,11]

Tissue engineering, in combination with novel biofabrication strategies, is a promising solution to engineer auricular implants with patient-derived donor cells.[12–15] These biofabricated auricular constructs could ultimately function as patient-specific implants for the reconstruction of a deformed auricle.

Successful engineering of a clinically relevant auricular cartilage implant requires a scaffold that provides a three-dimensional (3D) environment to support cell and tissue

Additional Supporting Information may be found in the online version of this article.
Correspondence to: D. O. Visscher; e-mail: d.visscher@vumc.nl
Contract grant sponsor: Dutch Burn Foundation; contract grant number: 15.107

growth. The optimal scaffold ideally matches the native properties of cartilage extracellular matrix (ECM) and is mechanically strong, porous, and biodegradable.[16,17] Unfortunately, creating such a construct is still a major challenge in the field of tissue engineering. In addition, efforts to translate engineered cartilage to the clinic have been hampered by problems associated with scaling up.[18] 3D printing can aid in both the production of 3D scaffolds that closely mimic the ECM of cartilage in terms of biomechanical properties and in producing larger, anatomically shaped tissues such as whole auricles. One strategy to engineer cartilage using 3D printing is to directly deposit the cells in a layer-by-layer fashion. The "bioink" that is required to directly deposit such cells consists of a synthetic, or more commonly, natural hydrogel mixed with cells.[19] Although hydrogels can closely resemble the native ECM of cartilage, the mechanical strength of such gels is low.[20] Therefore, hydrogels often require a synthetic supporting scaffold or microfibers that temporarily increase the mechanical properties.[21,22] These supporting scaffolds can be co-printed with the hydrogel to form an integrated scaffold construct.

Another common strategy to engineer cartilage using 3D printing is to print the supporting scaffold and manually load the cell-hydrogel mixture onto the 3D-printed scaffold, traditionally known as "top-down" approach.[23] Using this strategy, cells must deposit their own ECM on the prefabricated scaffold. A commonly used polymer for creating such a supporting scaffold is poly-ε-caprolactone (PCL). PCL is a promising biopolymer for tissue engineering due to its tuning possibility, chemical versatility, and strength,[24] and has been used in a clinical setting.

In a previous study, our group introduced the cage construct.[25] In that study, we developed a 3D-printed construct with a central core consisting of a natural polymer with cells, and an outer synthetic PCL cage for mechanical support. In the current study, we aimed to take this construct one step further by creating a clinically relevant and simplified two-part scaffold construct that can be easily assembled in the shape of human auricular cartilage. First, we tested the mechanical properties of both 3D printed PCL scaffolds and alginate hydrogel beads and discs and tested the survival of isolated chondrocytes inside the gel alone, with and without additional chondrogenic stimulation. Subsequently, we combined the two concepts by designing and 3D printing a two-part PCL mold in the shape of human auricular cartilage and injected this construct with a mixture of alginate and chondrocytes before culturing the final construct in vitro.

METHODS

Cell isolation and culture

Cell expansion. Cell isolation and culture of chondrocytes was performed as described previously.[25] Briefly, cartilage was obtained from the ears (n = 4) of sacrificed Dutch milk goats acquired from a local abattoir. The dissected cartilage was treated with 0.2 wt % type II collagenase (Roche diagnostics, Almere, the Netherlands) under gentle agitation at 37°C for 16 h to isolate the chondrocytes from the cartilage tissue. The digested tissue was subsequently filtered using a 40 μm-mesh to remove residual ECM, pelleted using centrifugation, and washed with PBS. The resulting cell suspension was cultured in GIBCO Dulbecco's modified Eagle's medium (DMEM; Life Technologies, Thermo Fisher Scientific, Waltham, MA, USA) supplemented with 10% fetal bovine serum (FBS; Hyclone-Thermo Scientific, Thermo Fisher Scientific, Waltham, MA, USA), 1% PSF (10,000 U/mL Penicillin, 10 mg/mL Streptomycin, 25 mg/mL Amphotericine B (Fungizone; Millipore Sigma, St. Louis, MO, USA), and 50 μg/mL L-(+) ascorbic acid (Merck, Darmstadt, Germany) (proliferation medium). When cell cultures reached 80% confluence, chondrocytes were trypsinized using 0.05% trypsin–EDTA, resuspended in cryoprotective medium (Recovery Freezing Medium, Life Technologies, Thermo Fisher Scientific, Waltham, MA, USA), and stored in liquid nitrogen until further use. All chondrocytes taken from liquid nitrogen were cultured up to passage three (P3) in proliferation medium to allow sufficient cells for three-dimensional (3D) culture in alginate hydrogel.

3D culture in alginate hydrogel beads. Sterile alginate solution was prepared by dissolving ultrapure sterile sodium alginate (MW 150–250 kDa, Pronova SLG100, Novamatrix, FMC Biopolymer, Sandvika, Norway) in 0.9 wt % Sodium Chloride (NaCl). The resulting alginate solution was vortexed at high speed and subsequently kept at room temperature for at least 1 h to minimize bubbles in the solution. For 3D alginate culture, cultured auricular chondrocytes were slowly suspended at a density of 4×10^6 cells/mL in 3 wt % alginate solution and transferred into 10 mL sterile syringe. The suspension was slowly passed through a 21-gauge (21G) needle to produce small drops, which fell into a sterile 102 mM $CaCl_2$ solution to allow instantaneous gelation. Following gelation, the beads were allowed to further gelate for 10 min in $CaCl_2$ solution before being washed with 0.9 wt % NaCl and transferred to a 24-well plate.

Beads were cultured in either proliferation medium (as described in *Cell Expansion*) or chondrogenic medium. Chondrogenic medium consisted of DMEM supplemented with 1% FBS, 1% PSF, 50 μg/mL L-(+) ascorbic acid, with added 1× Insulin Transferrin Selenium (ITS, Sigma-Aldrich) and 10 ng/mL transforming growth factor β1 (TGF-β1; R&D systems, Minneapolis, MN). Beads were cultured in vitro for 21 days and processed for LIVE/DEAD (Thermo Fisher Scientific, Waltham, MA) analysis, (immuno)histological analysis, and biomechanical analysis. Culture medium was changed twice a week.

PCL scaffold design and fabrication

PCL scaffolds. Three-dimensional scaffolds with five different distances between strands (400 μm, 600 μm, 800 μm, 1000 μm, and 1200 μm) were designed using an in-house custom software that generated 3D-printing control code (G-code) and printed using PCL on a 3DDiscovery printer (RegenHU, Switzerland). Medical-grade PCL (Purasorb PC12; Corbion, Purac Biomaterials) was extruded (HM-300H thermo polymer extruder, RegenHU; extrusion rate 18 revolutions/m) through a preheated needle (ø300 μm; 80°C) at

0.2 MPa (2 bar) and plotted in a layer-by-layer fashion at 5 mm/s. For smaller porosities, the extrusion rate was adjusted to ensure open porosity.

Auricular cartilage mold. An auricular cartilage mold, based on the parametric model described in the study by Bos et al.,[26] was designed in CATIA V5 software (Dassault systemes, Vélizy-Villacoublay, France). The two-part mold was processed in the custom software (see above) to obtain a controllable G-code for 3D printing. Using the optimal porosity from the above experiment, the auricular mold was then printed in two parts on the 3DDiscovery printer using the same settings as described previously. Following 3D printing, the molds were disinfected in 70% ethanol for 1 h, washed 3 times with sterile PBS, and air-dried in a sterile incubator. Following disinfection, all mold parts were transferred to individual petri dishes and coated with sterile gelatin (10%, Merck KGaA, Darmstadt, Germany) to block the pores and generate a sealed mold. After gelation of the gelatin solution at room temperature, 400 µL of the cell-alginate mixture (same suspension as described in 3D culture in alginate hydrogel beads) was injected into the bottom part of the mold, crosslinked for 2 min using 102 mM $CaCl_2$, and directly closed by placing the top part of the mold. Upon subsequent immersion into proliferation medium at 37°C, the gelatin liquefied and vacated the pores to allow nutrient and oxygen exchange through the mold pores. Figure 1A provides a complete overview of the fabrication process. The complete auricular implant models (Fig. 1B) were cultured in vitro in proliferation medium at 37°C, 5% CO_2 for 21 days and processed for LIVE/DEAD staining.

Microscopy

Optical microscopy (5× Objective, Nikon Eclipse LV100ND, Tokyo, Japan) was performed to assess the microscopic architecture of the 3D printed PCL scaffolds. Scaffolds were imaged from the top, bottom, and side view and processed in accompanying software (NIS-Elements, Nikon). The overall structure of the 3D printed PCL scaffolds was assessed with a stereoscopic microscope (Nikon SMZ-10) with a digital camera (Nikon DXM1200F) and fiber optic light source (Schott, KL1500-T).

A Light sheet microscope (UltraMicroscope II, LaVision BioTec GmbH, Bielefeld, Germany) equipped with a white light laser (SuperK EXTREME, NKT photonics; excitation 400–800 nm) and cMOS camera (Neo, Andor) and a Nikon Eclipse 80i confocal microscope were used to image *chondrocyte-laden* alginate beads and *chondrocyte-laden* alginate taken out of the auricular implant model respectively. The beads were placed in a holder and submerged in PBS during imaging. In general, the light sheet microscope has good optical sectioning capabilities allowing *Z*-plane imaging of intact hydrogels. However, light only penetrates a few hundred micrometers into transparent tissues.[27]

Cell viability analysis and quantification

A LIVE/DEAD viability/cytotoxicity kit (L3224; Thermo Fisher Scientific) was used to assess cell viability in *chondrocyte-laded* alginate beads according to manufacturer's instructions. Briefly, *chondrocyte-laden* alginate beads were washed in PBS, followed by incubation in 0.5 µL/mL Cal-AM and 2 µL/mL Eth-D (Thermo Fisher) in PBS at 37°C for 1.5 h. Beads were washed again in PBS and imaged using light sheet or confocal microscopy. Live and dead cell

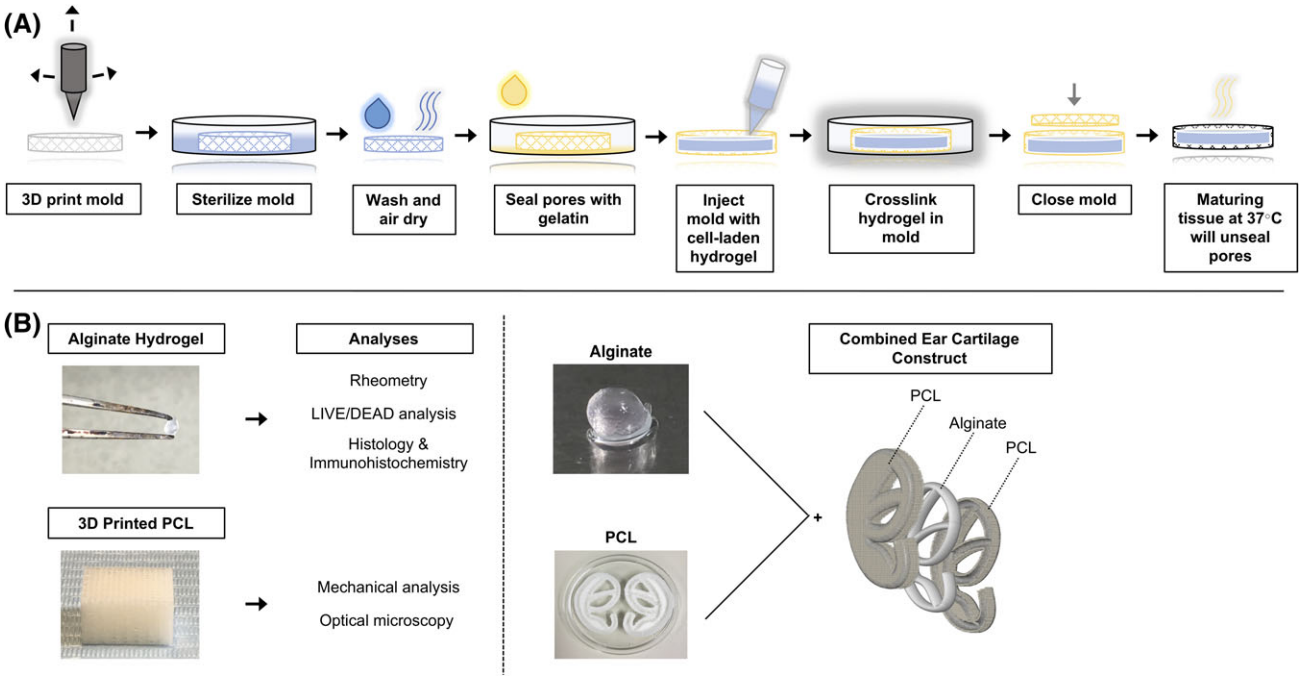

FIGURE 1. (A) Schematic of steps in the biofabrication of the implant model. (B) Schematic of the study methods. First, alginate hydrogel beads and 3D-printed PCL scaffolds were analyzed individually. Next, alginate and PCL were combined in one construct to develop an auricular implant model. PCL: Poly-ε-caprolactone.

quantification was performed in ImageJ v1.47 for Mac using the "process > find maxima" function.

Cell quantification in alginate beads cultured in proliferation and chondrogenic medium was performed using DAPI staining. Unfixed *chondrocyte-laden* alginate beads were covered in Tissue-Tek, snap frozen, and cut in 20 μm sections using a cryostat. Following the application of mounting medium (Fluoroshield Mounting Medium with DAPI; Abcam), beads (n = 3 per group) were imaged on a Nikon Eclipse 80i confocal microscope. Cells were counted in NIS-Elements AR software (v 3.2; Nikon Instruments Europe B.V). Both the total number of cells and percent (%) cells per bead were calculated per section.

Histology and immunohistochemistry

For histology and immunohistochemistry (IHC), unfixed *chondrocyte-laden* alginate beads were covered in Tissue-Tek (Thermo Fisher), snap frozen in liquid nitrogen, and cut in 14–20 μm sections at −20°C using a cryostat. Sections were mounted on Superfrost Plus Gold microscopic slides (Thermo Scientific) and stained with Alcian Blue (pH 1.0) for histological examination or processed for IHC. For IHC, sections were incubated for 2 h with monoclonal antibodies against type II collagen (II-II6B3, Developmental Studies Hybridoma Bank) or type VI collagen (MAB3303, EMD Millipore). Following incubation, sections were washed in PBS and incubated for 30 min with EnVision (Dako). Finally, sections were incubated with AEC substrate for 10 min and visualized using microscopy. Postprocessing was undertaken using NIS Elements software (Nikon Instruments Europe B.V.).

Control cartilage samples derived from goat ears were embedded in paraffin using standard histological techniques, cut in 5 μm sections, and stained using Alcian Blue, Mayer's Hematoxylin-Eosin, type II and type VI collagen to assess glycosaminoglycan distribution, morphology, and

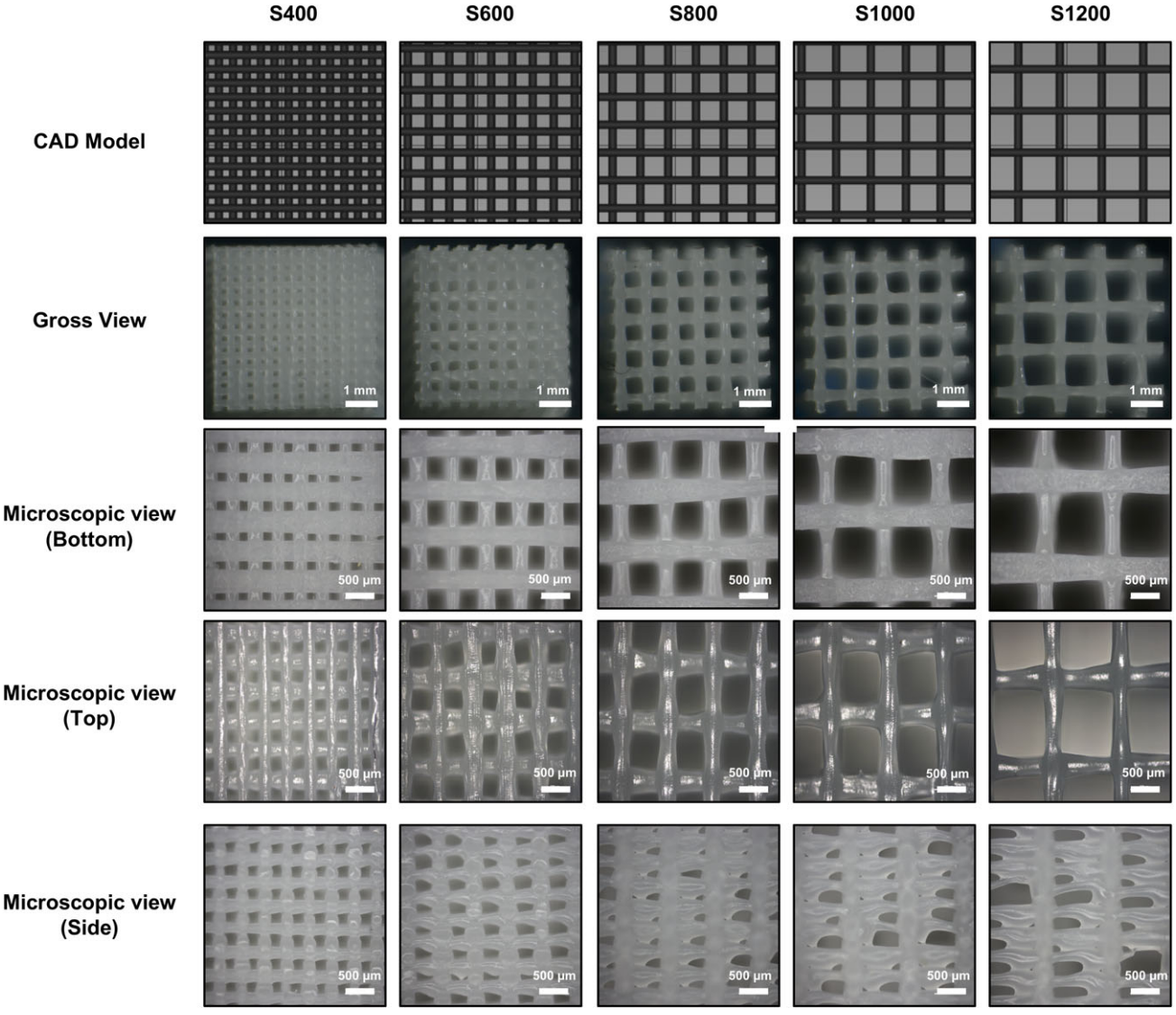

FIGURE 2. CAD view, gross view, and microscopic views of 3D-printed PCL scaffolds with varying distances between strands. S represents the sample, with the number representing the distances between strands in micrometers (μm).

collagen distribution, respectively (Supporting Information Fig. S1).

(Bio)mechanical analysis

PCL scaffolds. The mechanical properties of PCL scaffolds with varying *distances between strands* (400–1200 μm; n = 5 per group) were analyzed using mechanical compression testing according to the ASTM standard D695. The 3D-printed PCL blocks were cut into six cuboids (5 mm wide × 5 mm wide × 10 mm high) using a new blade for each sample. An Instron 5969 machine with a 5 kN load cell was used to compress unconstrained samples between two steel plates at a rate of 1 mm min^{-1} to 33% strain. Five samples were tested for each scaffold design (porosity). Compressive moduli were calculated for all samples using a linear-elastic compression phase as the applied force increased from 10 to 50 N.

Alginate hydrogel. For mechanical characterization of empty and *chondrocyte-laden* alginate beads after in vitro cell culture, compression was performed using a Physica MCR 501 rheometer (Anton Paar, GmbH, Austria). The gap between the plates was lowered from 2 mm to 0.1 mm at a rate of 0.001 mm s^{-1} and the resulting normal force from the sample on the top plate was recorded. To determine the storage (G') and loss (G") shear moduli, small-amplitude oscillatory shear (SAOS) rheometry at a frequency of 0.5 Hz and with a strain amplitude of 0.5% was performed on 2 mm (height) × 20 mm (diameter) *chondrocyte-laden* alginate disks that were created using a 3D printed mold. All samples were tested at 37°C using PP20 stainless steel geometry (parallel plates, 20 mm diameter).

Statistical analysis. Data were analyzed using GraphPad Prism version 6.02 (Graphpad Software). Data are represented as Mean ± Standard Deviation (SD) unless otherwise indicated. Statistical analysis was performed using unpaired t-tests or one-way analysis of variance (ANOVA) with multiple comparisons. Chondrocytes proliferation and storage/loss modulus of *chondrocyte-laden* alginate beads and disks were analyzed using unpaired *t*-tests, while ANOVA was used for comparing the compressive moduli of 3D printed PCL scaffolds. A p value of <0.05 was considered statistically significant.

RESULTS

Structural properties of 3D-printed PCL. The structural properties of 3D-printed PCL scaffolds were determined by examining the surface porosity and mechanical properties. Macroscopic analysis of the PCL scaffolds showed good printing quality (Fig. 2, gross view). However, microscopic analysis of individual PCL strands showed some variance in

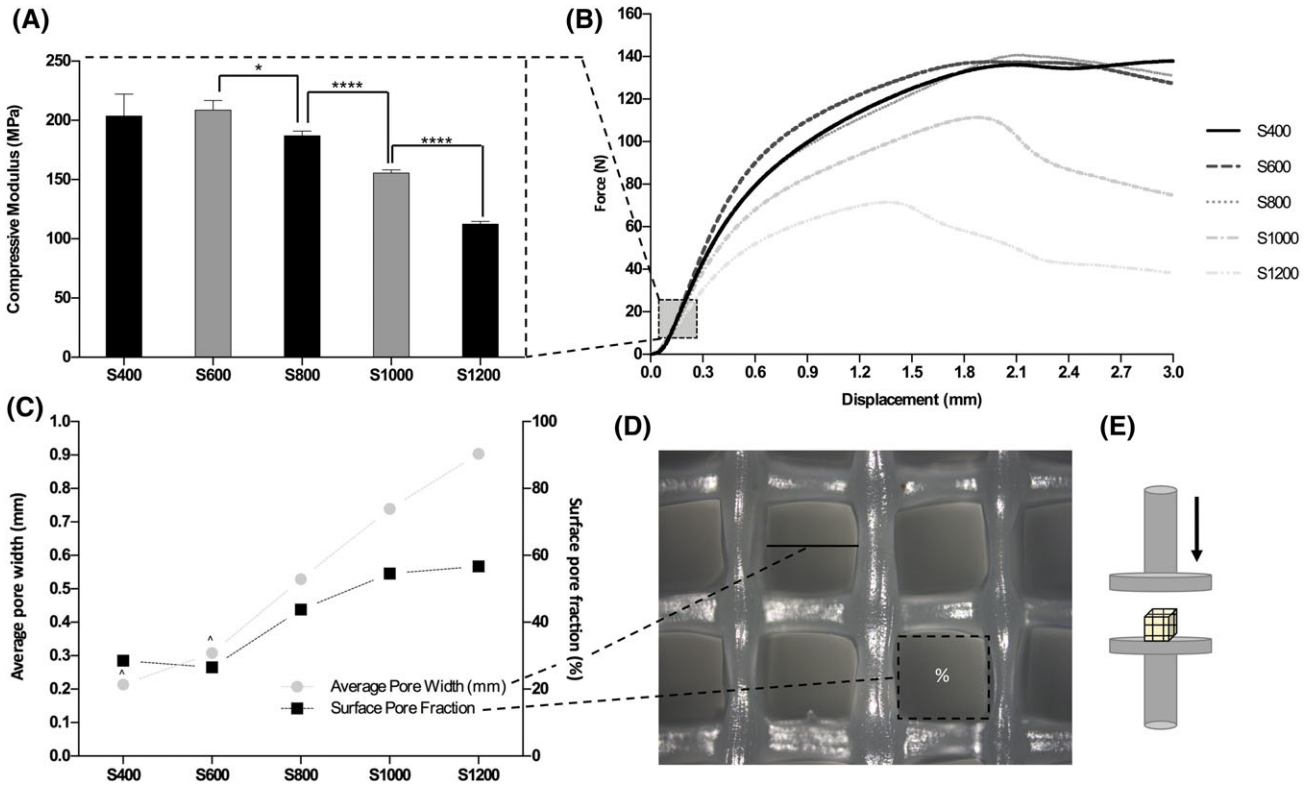

FIGURE 3. Mechanical analysis and pore size analysis of 3D-printed PCL scaffolds with varying distances between strands. (A) Mean compressive modulus (MPa) of PCL scaffolds with varying porosities. $S_{(number)}$ = sample $_{(distance\ between\ strands)}$. (B) Force – displacement curves of PCL scaffolds with varying porosities. (C) Average pore width (mm) and surface pore fraction (0–1) of 3D-printed PCL scaffolds. To allow for open porosity, the S400 and S600 scaffolds were printed using a lower extrusion rate (10 and 15 revs/m, respectively). (D) Illustration of pore (mm) width and surface pore fraction (%) measurement. (E) Direction of axial compression of PCL scaffolds. $^{*}p < 0.05$, $^{****}p < 0.001$.

strand diameter over a short distance (Fig. 2, microscopic view). In addition, the lateral view of the scaffold showed a large variety in pore width (Fig. 2, side view). Overall, the smaller the pore width, the more accurate the 3D-printed scaffold. Specifically, the S400 and S600 showed qualitatively more repeatable pores than S800-S1200 (Fig. 2).

The compressive modulus was highest in the scaffolds with the smallest pore fraction (Fig. 3A). The compressive modulus of S600 and S800 did not significantly differ from S400 (p = 0.91 and p = 0.07, respectively). To ensure pores were not blocked, the S400 and S600 scaffolds were printed with lower extrusion rates (decreasing the overall strand thickness) of 10 and 15 revs/m, respectively, as opposed to 18 revs/m for other samples. This may have caused a slight decrease in compressive modulus, as well as increase in surface pore fraction (Fig. 3C). Nevertheless, there was an overall trend that the higher the pore size and pore fraction, the lower the mechanical properties. The surface pore fraction however, calculated as the percentage of open space versus total area (Fig. 3D), was notably lower in scaffolds with smaller pores (Fig. 3C): the surface pore fraction of S400 and S600 were approximately 30%, whereas the surface pore fraction of S1000 and S1200 reached approximately 50% (Fig. 3C).

Cell viability and proliferation in alginate hydrogel beads. *Chondrocyte-laden* alginate hydrogel beads were evaluated for cell survival and proliferation after 21 days of cell culture. In proliferation medium, cells displayed a rounded morphology and were dispersed throughout the alginate hydrogel beads, with more cells found at the edges of the beads (Figs. 4A and 5A). In chondrogenic medium, cells were also dispersed throughout the alginate, but in multiple cell clusters (Figs. 4A and Fig. 5B). Cell survival was high in both proliferation and chondrogenic medium (82.67% ± 2% and 82.40% ± 2%, respectively, p = 0.88, Fig. 4B). Both the total number of cells (Fig. 5C), and area of cells (%) were higher in beads cultured in chondrogenic medium compared to proliferation medium ($p < 0.05$).

Hydrogel biomechanical properties. The biomechanical properties of *chondrocyte-laden* alginate hydrogels (beads and discs) were tested using compression tests and SAOS rheometry. The overall normal force of the *chondrocyte-laden* alginate beads following compression is shown in Fig. 6A. Beads cultured in proliferation medium exerted higher forces (0.24 N) at 1 mm gap (~50% strain) than control beads (without cells) (0.06 N) and beads cultured in chondrogenic medium (0.07 N) following a culture period of 21 days.

We next tested the elastic shear modulus (G') of *chondrocyte-laden* alginate disks after 28 days of culture in different culture media. The elastic modulus of discs cultured in proliferation medium (6100 ± 1925 Pa) was higher than the elastic modulus of discs cultured in chondrogenic medium (3423 ± 1092 Pa), although the difference was

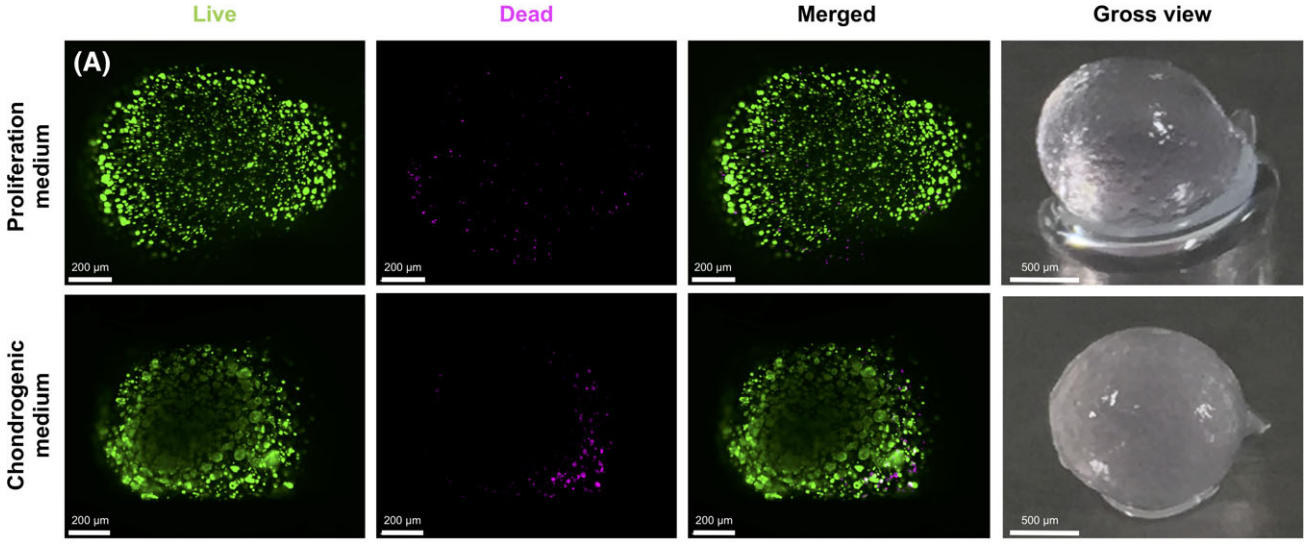

(B) Culture Medium	% Live	% Dead
Proliferation	82.67 ± 2.24 %	17.67 ± 1.95 %
Chondrogenic	82.40 ± 1.68 %	17.60 ± 1.68 %
P-value	P = 0.88	P = 0.96

FIGURE 4. (A) Representative LIVE/DEAD stains of alginate beads with chondrocytes after 21 days of culture in "proliferation" medium and "chondrogenic" medium (additional TGF-β and ITS premix). Green represents live cells, magenta represents dead cells. Blurring in the center of the "chondrogenic" alginate bead is due to limited light penetration in the 3D construct. (B) Quantification of live and dead cells in alginate beads cultured in "proliferation" and "chondrogenic" medium.

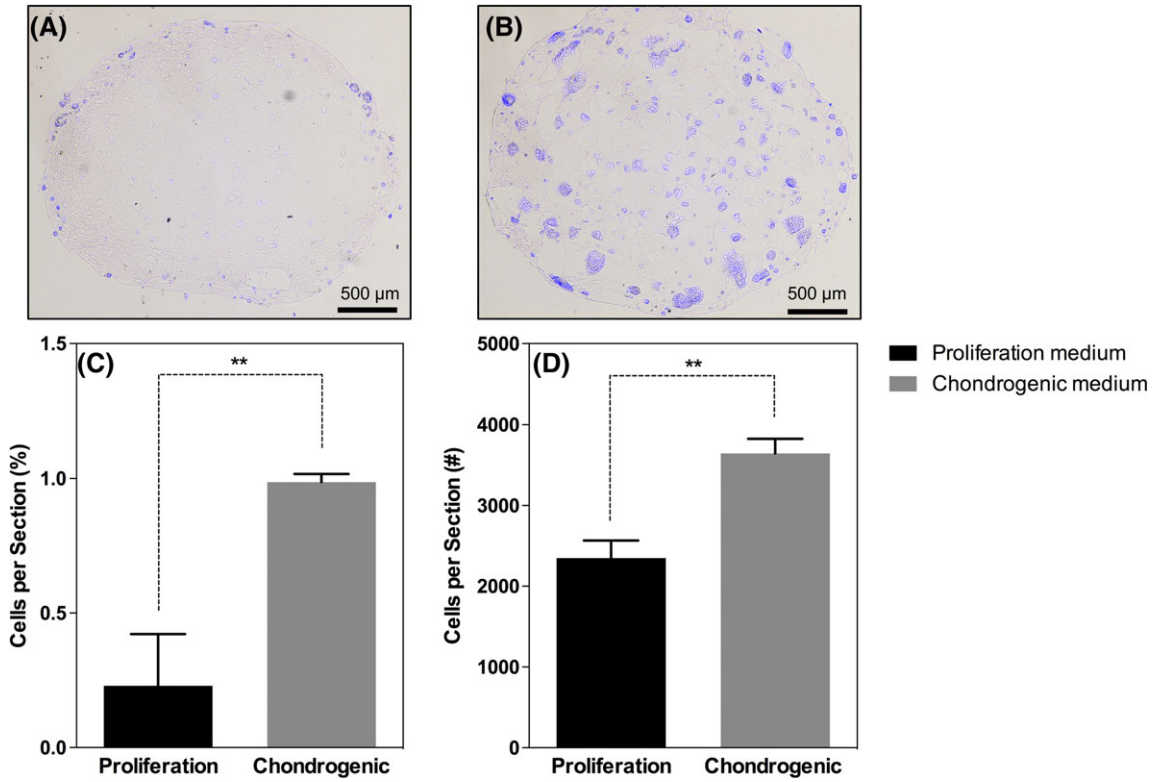

FIGURE 5. Chondrocyte proliferation after 21 days of culture in proliferation and chondrogenic medium. (A) DAPI stain of alginate bead in proliferation medium (cryosection; 20 μm). (B) DAPI stain of alginate bead in chondrogenic medium (cryosection; 20 μm). **C)** Mean ± SD of cells per section (%) in proliferation and chondrogenic medium. (D) Mean ± SD of cells per section (#) in proliferation and chondrogenic medium. n = 3, $^{**}p < 0.05$.

not statistically significant ($p = 0.104$), Figure 6B. Alginate discs without cells cultured in proliferation medium showed an average elastic modulus of 4163 ± 1111 Pa (Fig. 6B).

Neocartilage formation. The production of glycosaminoglycans, type II collagen, and type VI collagen were assessed in *chondrocyte-laden* alginate beads (Fig. 7). In proliferation medium, chondrocytes deposited some pericellular and territorial glycosaminoglycans, while in chondrogenic medium, there was pericellular, territorial, and interterritorial deposition of glycosaminoglycans. Native auricular cartilage showed mostly pericellular and territorial glycosaminoglycans, with some interterritorial glycosaminoglycans (Supporting Information Fig. S1).

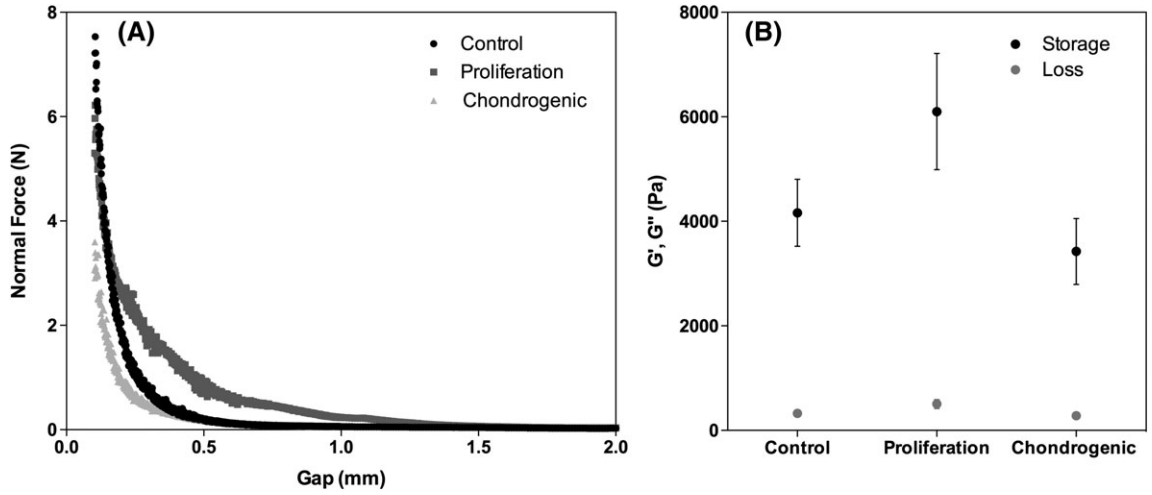

FIGURE 6. (A) Normal force of control beads and alginate beads cultured in proliferation and chondrogenic medium. n = 3, no statistically significant differences found ($p > 0.05$) between control disks, and disks cultured in proliferation and chondrogenic medium. (B) Mean ± SEM of storage and loss modulus in control alginate disks and chondrocyte-laden disks cultured in proliferation and chondrogenic medium for 28 days.

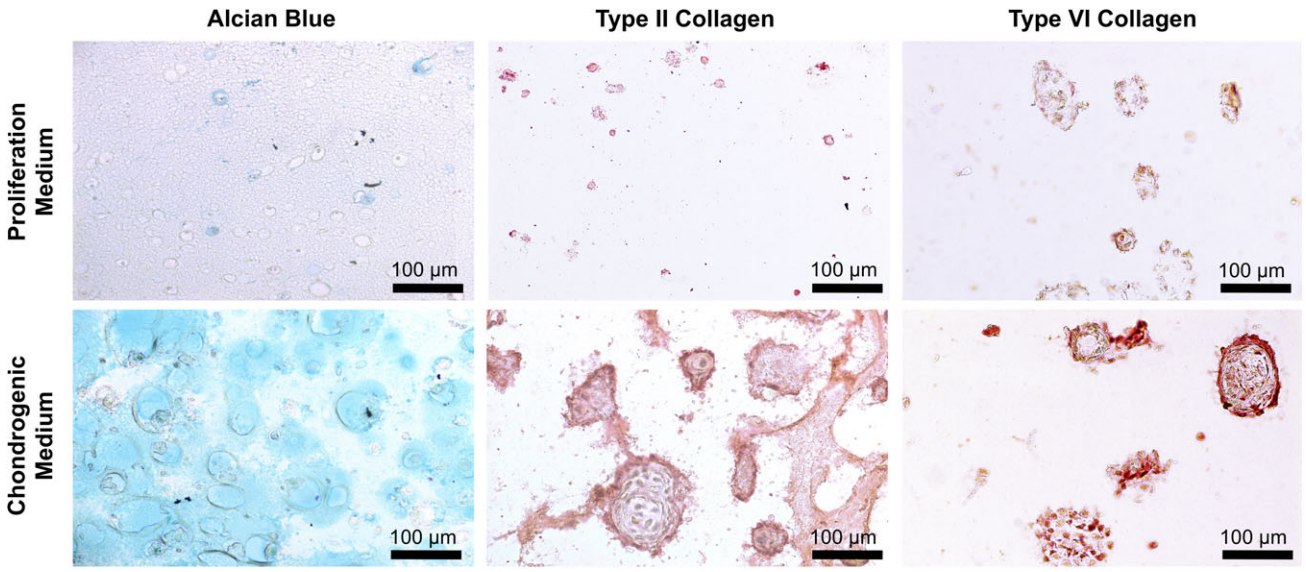

FIGURE 7. Histological and Immunohistological analysis of chondrocyte-laden alginate beads.

After 21 days, type II collagen produced by chondrocytes in beads cultured in proliferation medium was deposited mostly in the pericellular region. Chondrogenic medium stimulated some additional deposition in territorial and interterritorial regions (Fig. 7). Type VI collagen deposition was mostly pericellular in both proliferation and chondrogenic medium. However, large cell clusters in chondrogenic medium seemed to have formed some territorial matrix. In native auricular cartilage, type VI collagen, although most dense in the pericellular/territorial region, appeared rather dispersed throughout the whole tissue (Supporting Information Fig. S1).

Auricular implant model. To assess the feasibility of developing an auricular implant model, both PCL and alginate were combined in one construct. From the above

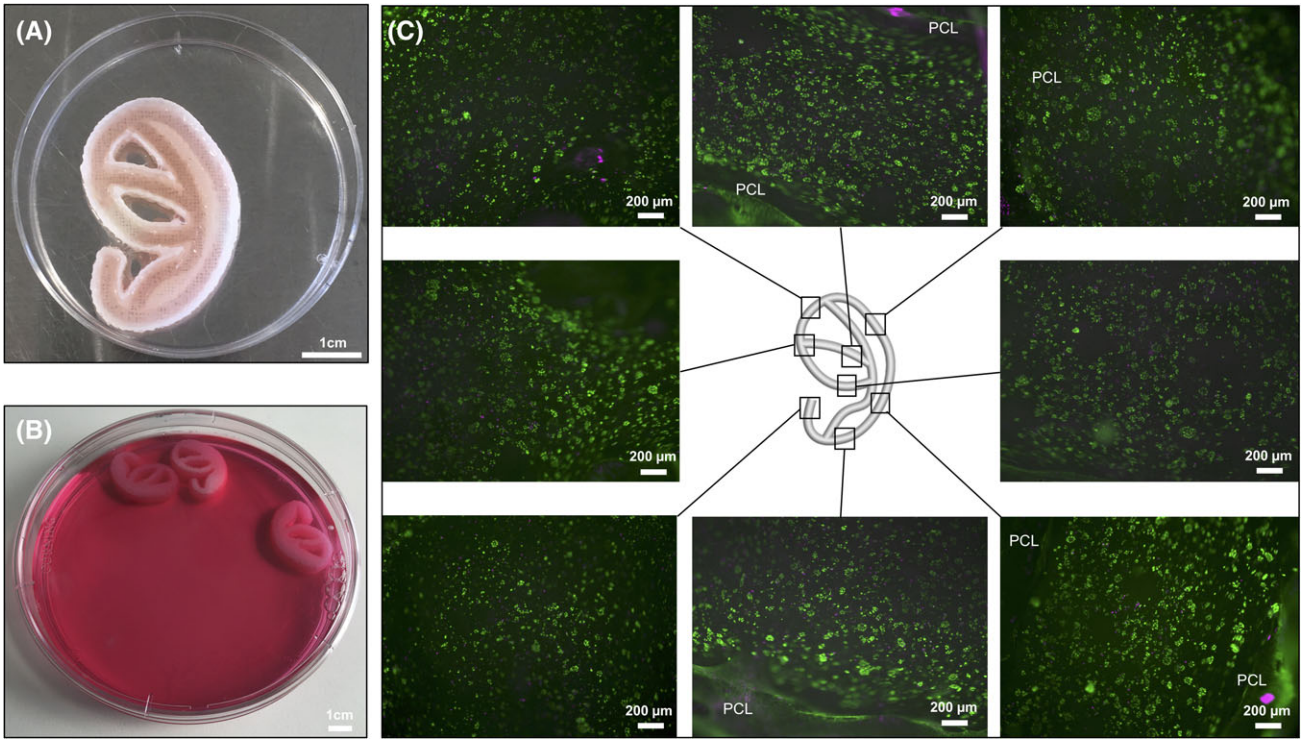

FIGURE 8. (A) Gross view of the PCL-alginate auricular implant model. Alginate can be found inside the grooves of the PCL mold. Note that one part of the 2-part mold has been taken off for viewing. (B) in vitro cultured PCL-alginate auricular implant models. (C) LIVE/DEAD stain of alginate taken out of the PCL mold after 21 days of culture. High-cell survival was seen throughout the entire implant model.

experiments (Figs. 2 and 3), a porosity of 300 μm (S600) was chosen for the auricular implant model because it demonstrated both a high compressive modulus and repeatable pore geometry. The two-part auricular mold (Figs. 1 and 8A, B) could be printed with high fidelity. The final size of the assembled PCL mold was 40 mm (height) × 25 mm (width) × 6 mm (thickness). After the in vitro culture period in proliferation media for 21 days, the top mold could be removed easily without alginate sticking to the PCL. After removal (Fig. 8A), the alginate was seen to be evenly distributed in the grooves of the PCL mold. The size of the mold did not change during in vitro culture. Cell survival was high (>85%) in the alginate gel after 21 days of culture at all positions in the construct (Fig. 8C). The cells preferred the alginate as microenvironment as opposed to the surrounding PCL; very few cells attached to the PCL scaffold. Furthermore, cells were distributed evenly both throughout the model and in the alginate hydrogel.

DISCUSSION

Advances in the field of tissue engineering and biofabrication provide a possibility to overcome current issues in auricular cartilage reconstruction. One of these issues is creating an implant model that both mimics the complexity of the auricle and maintains this complexity during cellular growth and tissue remodeling. In the current study, we developed and tested a biofabricated auricular implant model in vitro, that can be used for ear reconstruction.

Appropriate selection of the biomaterials is vital for the long-term success of implants.[28] In this study, PCL was used because of its inherent strength for potential subcutaneous in vivo implantation,[13] high elasticity,[29,30] and low-melting temperature of 60°C, making it an excellent biomaterial for 3D printing.[31] 3D-printed PCL scaffolds exhibited very high-compressive moduli (100–200 MPa), depending on the porosity (Fig. 3A).[32] These compressive moduli are approximately 100 times higher than that of native auricular cartilage,[33,34] and are similar to the clinical synthetic implant material porous polyethylene (Medpor),[10,34] which is widely used for auricular reconstruction.[3,35] The high stiffness of the PCL is both advantageous for protection of the hydrogel as well as shape preservation following possible implantation.[36]

Scaffold porosity is an important aspect in biofabrication-based tissue engineering.[37] For example, Medpor constructs, with pores greater than 100 μm, allows soft tissue and vascular ingrowth when implanted in patients.[38] We found the optimal porosity in terms of mechanical properties, 3D design, and PCL material, to be 300 μm (S600) (Fig. 3C). Although, 3D-printed scaffolds with smaller pore sizes (S400) seemed more accurate (Fig. 2), some pores were blocked, which would be expected to block nutrient diffusion in the hydrogel. In addition, smaller pore sizes have been shown to promote less tissue ingrowth than larger pores.[39]

With regards to nutrient diffusion in the alginate hydrogel, beads cultured in both proliferation medium and chondrogenic medium displayed high cell survival after 21 days in vitro (~83%). There are various reasons why cell survival is not 100%, including chemical crosslinking with calcium chloride,[40] alginate viscosity,[41] and cell culture conditions.[42] Stimulation with chondrogenic medium did not increase the percentage of cell survival but did significantly increase cell proliferation and cluster formation (Fig. 5). Cell cluster formation in 3D hydrogels has been shown previously,[43–45] but the mechanism by which cell clusters are formed is poorly understood.[46] Cell clustering could be induced by stimulation with TGF-beta present in our chondrogenic medium. However, this phenomenon is mostly seen in osteoarthritic models.[47,48] Nevertheless, a study by Cavo and colleagues[49] showed that MCF-7 cells show high-cell proliferation, associated with cluster formation, in soft alginate hydrogels. In addition, Mhanna and colleagues[50] explain that alginate inhibits cell migration and forces cells to proliferate in nodes resulting in cell clusters. In this study, the compressive modulus of alginate beads stimulated with chondrogenic media was lower while the proliferation rate was higher. Therefore, proliferation rate might not only be related to hydrogel stiffness, but also cluster formation.

The stiffness of in vitro cultured *chondrocyte-laden* alginate beads was low (~5 kPa, Fig. 6B) compared to native auricular cartilage (~1 MPa[34]). Although not statistically significant, there was a noticeable difference in the elastic modulus of beads cultured in proliferation medium (~6 kPa) compared to chondrogenic medium (~3.5 kPa). Although, we expected that stimulation with TGF-beta would increase the mechanical properties of the beads by increasing chondrocyte proliferation and matrix synthesis, the opposite was found. This negative effect of continuous TGF-beta stimulation has also been shown by others,[51–53] which could suggest that transient exposure of TGF-beta is important to improve tissue formation.[52]

A study by Bhujbal and colleagues[42] identified several factors that may influence the overall mechanical stability of alginate beads, including storage solution and cell load. They showed that the mechanical properties of beads cultured in DMEM decreased significantly. This might also explain the low elastic moduli of our *chondrocyte-laden* alginate beads in vitro. In addition, higher cell load could explain a lower elastic modulus in *chondrocyte-laden* alginate beads stimulated with TGF-beta (Fig. 5).

ECM deposition was more prominent in *chondrocyte-laden* alginate beads cultured in chondrogenic medium. Both glycosaminoglycans and type II collagen deposition were higher in beads cultured in chondrogenic medium, which is consistent with previous data.[54–56] To determine whether the pericellular matrix of auricular chondrocytes was affected by TGF-beta stimulation, we performed type VI collagen immunostaining. Type VI collagen was weakly positive in the pericellular regions of both chondrocytes stimulated with proliferation and chondrogenic medium, which is consistent with a previous study on auricular cartilage macroaggregates.[57] However, native auricular cartilage stained highly positive for VI collagen in both pericellular and territorial matrix (Supporting Information Fig. S1).

Finally, to test the feasibility of printing an auricular implant model that is easily injectable with hydrogel, we combined both PCL and alginate in one construct. There are numerous approaches to biofabrication-based auricular reconstruction, most of which use a combination of hydrogels and thermoplastic polymers.[14,15,58] Although, we also used a combination of these materials, we applied a novel approach by creating a two-part biodegradable 3D-printed mold made from PCL that is easily assembled and injectable using any type of hydrogel. Injected alginate allowed high cell survival after 21 days of culture in the auricular mold (Fig. 8). Auricular mold designs have been used previously by other groups, but were difficult to fabricate and were not integrated in the final engineered auricular tissue.[7,36,51] The novel hybrid implant model presented in this study may have several advantages over other scaffold designs: (1) PCL, which can cause inflammation when implanted in vivo,[24] will not be present in the maturing tissue, which in this design is found inside the mold, (2) the mold design can have very high mechanical properties without affecting the mechanical properties of the maturing tissue, (3) the mold design can be easily retrieved and disassembled after in vivo maturation[59] as the mold offers a partial barrier between the maturing tissue and native tissue, and (4) if necessary, the properties of the PCL mold could be adjusted to decrease the degradation rate, which can normally take up to 24 months.[24] Making use of these advantages, the mold design could then be used as follows: (1) mold assembly, (2) in vivo implantation, (3) tissue maturation, (4) retrieval of the implant model, (5) disassembly of the outer mold, (6) reconstruction using the matured cartilage tissue. Although, the auricular implant model in this study was injected with *chondrocyte-laden* alginate, the mold construct could be injected with any other type of hydrogel and cell source, for example, with hydrogels based on decellularized cartilage tissue.[60–62]

CONCLUSION

Here, we have described the process for engineering of a hybrid auricular cartilage implant model for facial reconstruction (see Fig. 1A). The hybrid implant model consists of a porous synthetic outer mold with high mechanical properties required to overcome forces during in vivo tissue maturation, and an inner "natural" core that consists of a biomimetic environment for cartilage tissue formation. The mold can be easily printed and assembled, while the design makes it easy to inject any suitable hydrogel for tissue formation. While long-term in vivo experiments are required to test its preclinical applicability, the work presented in this study provides a possible strategy for the use of biofabricated tissue constructs in the clinic.

ACKNOWLEDGMENTS

This work was financially supported by the Dutch Burn Foundation (project number 15.107). The authors would like to thank Mr. Sjoerd te Slaa and Mr. Niels Liberton for help with computer aided design. In addition, the authors acknowledge Nanne Paauw, Esther Hendrickx, and Sander Spiekstra for help with imaging of the alginate beads. The authors declare that they have no competing interests.

REFERENCES

1. Fernandes JR, Driscoll DN. Burn ear reconstruction using porous polyethylene implants and tissue expansion. J Burn Care Res Off Publ Am Burn Assoc 2016 Aug;37(4):e348–e352.
2. Ali K, Trost JG, Truong TA, Harshbarger RJ. Total ear reconstruction using porous polyethylene. Semin Plast Surg 2017 Aug;31(3): 161–172.
3. Kludt NA, Vu H. Auricular reconstruction with prolonged tissue expansion and porous polyethylene implants. Ann Plast Surg 2014 May;72(Suppl 1):S14–S17.
4. Olshinka A, Louis M, Truong TA. Autologous ear reconstruction. Semin Plast Surg 2017 Aug;31(3):146–151.
5. Soukup B, Mashhadi SA, Bulstrode NW. Health-related quality-of-life assessment and surgical outcomes for auricular reconstruction using autologous costal cartilage. Plast Reconstr Surg 2012 Mar; 129(3):632–640.
6. Chauhan DS, Guruprasad Y. Auricular reconstruction of congenital microtia using autogenous costal cartilage: report of 27 cases. J Maxillofac Oral Surg 2012 Mar;11(1):47–52.
7. Reiffel AJ, Kafka C, Hernandez KA, Popa S, Perez JL, Zhou S, Pramanik S, Brown BN, Ryu WS, Bonassar LJ, Spector JA. High-fidelity tissue engineering of patient-specific auricles for reconstruction of pediatric microtia and other auricular deformities. PLoS One 2013;8(2):e56506.
8. Nayyer L, Patel KH, Esmaeili A, Rippel RA, Birchall M, O'toole G, et al. Tissue engineering: revolution and challenge in auricular cartilage reconstruction. Plast Reconstr Surg 2012 May;129(5):1123–1137.
9. Lewin S. Complications after Total porous implant ear reconstruction and their management. Facial Plast Surg FPS 2015 Dec;31(6):617–625.
10. Nayyer L, Birchall M, Seifalian AM, Jell G. Design and development of nanocomposite scaffolds for auricular reconstruction. Nanomedicine 2014 Jan;10(1):235–246.
11. Romo T, Reitzen SD. Aesthetic microtia reconstruction with Medpor. Facial Plast Surg FPS 2008 Jan;24(1):120–128.
12. Otto IA, Melchels FPW, Zhao X, Randolph MA, Kon M, Breugem CC, Malda J. Auricular reconstruction using biofabrication-based tissue engineering strategies. Biofabrication 2015 Jul 22;7(3):32001.
13. Zopf DA, Mitsak AG, Flanagan CL, Wheeler M, Green GE, Hollister SJ. Computer aided-designed, 3-dimensionally printed porous tissue bioscaffolds for craniofacial soft tissue reconstruction. Otolaryngol--Head Neck Surg Off J Am Acad Otolaryngol-Head Neck Surg 2015 Jan;152(1):57–62.
14. Lee J-S, Hong JM, Jung JW, Shim J-H, Oh J-H, Cho D-W. 3D printing of composite tissue with complex shape applied to ear regeneration. Biofabrication 2014 Jun;6(2):24103.
15. Kang H-W, Lee SJ, Ko IK, Kengla C, Yoo JJ, Atala A. A 3D bioprinting system to produce human-scale tissue constructs with structural integrity. Nat Biotechnol 2016 Mar;34(3):312–319.
16. Geckil H, Xu F, Zhang X, Moon S, Demirci U. Engineering hydrogels as extracellular matrix mimics. Nanomedicine 2010 Apr;5(3): 469–484.
17. Hutmacher DW. Scaffolds in tissue engineering bone and cartilage. Biomaterials 2000 Dec;21(24):2529–2543.
18. Rustad KC, Sorkin M, Levi B, Longaker MT, Gurtner GC. Strategies for organ level tissue engineering. Organogenesis 2010 Sep;6(3): 151–157.
19. Murphy SV, Atala A. 3D bioprinting of tissues and organs. Nat Biotechnol 2014 Aug;32(8):773–785.
20. Zhu J, Marchant RE. Design properties of hydrogel tissue-engineering scaffolds. Expert Rev Med Devices 2011 Sep;8(5): 607–626.
21. Tibbitt MW, Anseth KS. Hydrogels as extracellular matrix mimics for 3D cell culture. Biotechnol Bioeng 2009 Jul 1;103(4):655–663.
22. Visser J, Melchels FPW, Jeon JE, van Bussel EM, Kimpton LS, Byrne HM, Dhert WJA, Dalton PD, Hutmacher DW, Malda J. Reinforcement of hydrogels using three-dimensionally printed microfibres. Nat Commun 2015 Apr 28;6:6933.
23. Nichol JW, Khademhosseini A. Modular tissue engineering: engineering biological tissues from the bottom up. Soft Matter 2009; 5(7):1312–1319.

24. Woodruff MA, Hutmacher DW. The return of a forgotten polymer—Polycaprolactone in the 21st century. Prog Polym Sci 2010 Oct; 35(10):1217–1256.
25. Visscher DO, Bos EJ, Peeters M, Kuzmin NV, Groot ML, Helder MN, van Zuijlen PPM. Cartilage tissue engineering: preventing tissue scaffold contraction using a 3D-printed polymeric cage. Tissue Eng Part C Methods 2016 Jun;22(6):573–584.
26. Bos EJ, Scholten T, Song Y, Verlinden JC, Wolff J, Forouzanfar T, Helder MN, van Zuijlen P. Developing a parametric ear model for auricular reconstruction: a new step towards patient-specific implants. J Craniomaxillofac Surg 2015 Apr;43(3):390–395.
27. Power RM, Huisken J. Adaptable, illumination patterning light sheet microscopy. Sci Rep 2018;8(1):9615.
28. Saini M. Implant biomaterials: a comprehensive review. World J Clin Cases 2015;3(1):52–57.
29. Gunatillake P, Mayadunne R, Adhikari R. Recent developments in biodegradable synthetic polymers. Biotechnol Annu Rev 2006;12: 301–347.
30. Ulery BD, Nair LS, Laurencin CT. Biomedical applications of biodegradable polymers. J Polym Sci Part B Polym Phys 2011 Jun 15; 49(12):832–864.
31. Kim BS, Jang J, Chae S, Gao G, Kong J-S, Ahn M, Cho DW. Three-dimensional bioprinting of cell-laden constructs with polycaprolactone protective layers for using various thermoplastic polymers. Biofabrication 2016 Aug 22;8(3):35013.
32. Olubamiji AD, Izadifar Z, Si JL, Cooper DML, Eames BF, Chen DXB. Modulating mechanical behaviour of 3D-printed cartilage-mimetic PCL scaffolds: influence of molecular weight and pore geometry. Biofabrication 2016 Jun 22;8(2):25020.
33. Nimeskern L, Pleumeekers MM, Pawson DJ, Koevoet WLM, Lehtoviita I, Soyka MB, Röösli C, Holzmann D, van Osch GJVM, Müller R, Stok KS. Mechanical and biochemical mapping of human auricular cartilage for reliable assessment of tissue-engineered constructs. J Biomech 2015 Jul 16;48(10):1721–1729.
34. Griffin MF, Premakumar Y, Seifalian AM, Szarko M, Butler PEM. Biomechanical characterisation of the human auricular cartilages; implications for tissue engineering. Ann Biomed Eng 2016 Dec; 44(12):3460–3467.
35. Storck K, Staudenmaier R, Buchberger M, Strenger T, Kreutzer K, von Bomhard A, Stark T. Total reconstruction of the auricle: our experiences on indications and recent techniques. Biomed Res Int 2014;2014:1–15.
36. Kamil SH, Vacanti MP, Aminuddin BS, Jackson MJ, Vacanti CA, Eavey RD. Tissue engineering of a human sized and shaped auricle using a mold. Laryngoscope 2004 May;114(5):867–870.
37. O'Brien FJ. Biomaterials & scaffolds for tissue engineering. Mater Today 2011 Mar;14(3):88–95.
38. Wellisz T. Clinical experience with the Medpor porous polyethylene implant. Aesthet Plast Surg 1993;17(4):339–344.
39. Nayyer L, Jell G, Esmaeili A, Birchall M, Seifalian AM. A biodesigned Nanocomposite biomaterial for auricular cartilage reconstruction. Adv Healthc Mater 2016 May;5(10):1203–1212.
40. Cao N, Chen XB, Schreyer DJ. Influence of calcium ions on cell survival and proliferation in the context of an alginate hydrogel. ISRN Chem Eng 2012;2012:1–9.
41. Kong HJ, Smith MK, Mooney DJ. Designing alginate hydrogels to maintain viability of immobilized cells. Biomaterials 2003 Oct; 24(22):4023–4029.
42. Bhujbal SV, Paredes-Juarez GA, Niclou SP, de Vos P. Factors influencing the mechanical stability of alginate beads applicable for immunoisolation of mammalian cells. J Mech Behav Biomed Mater 2014 Sep;37:196–208.
43. Wu Z, Su X, Xu Y, Kong B, Sun W, Mi S. Bioprinting three-dimensional cell-laden tissue constructs with controllable degradation. Sci Rep 2016;6(1):1–10.
44. Ouyang L, Yao R, Chen X, Na J, Sun W. 3D printing of HEK 293FT cell-laden hydrogel into macroporous constructs with high cell viability and normal biological functions. Biofabrication 2015 Feb 18; 7(1):15010.
45. Zhao Y, Yao R, Ouyang L, Ding H, Zhang T, Zhang K, Cheng S, Sun W. Three-dimensional printing of Hela cells for cervical tumor model in vitro. Biofabrication 2014 Sep;6(3):35001.
46. Joddar B, Garcia E, Casas A, Stewart CM. Development of functionalized multi-walled carbon-nanotube-based alginate hydrogels for enabling biomimetic technologies. Sci Rep 2016;6(1):1–12.
47. Lotz MK, Otsuki S, Grogan SP, Sah R, Terkeltaub R, D'Lima D. Cartilage cell clusters. Arthritis Rheum 2010 Apr 21;62(8):2206–2218.
48. Livne E. In vitro response of articular cartilage from mature mice to human transforming growth factor beta. Acta Anat (Basel) 1994; 149(3):185–194.
49. Cavo M, Fato M, Peñuela L, Beltrame F, Raiteri R, Scaglione S. Microenvironment complexity and matrix stiffness regulate breast cancer cell activity in a 3D in vitro model. Sci Rep 2016 Oct 13;6: 35367.
50. Mhanna R, Kashyap A, Palazzolo G, Vallmajo-Martin Q, Becher J, Möller S, Schnabelrauch M, Zenobi-Wong M. Chondrocyte culture in three dimensional alginate sulfate hydrogels promotes proliferation while maintaining expression of chondrogenic markers. Tissue Eng Part A 2014 May;20(9–10):1454–1464.
51. Rosa RG, Joazeiro PP, Bianco J, Kunz M, Weber JF, Waldman SD. Growth factor stimulation improves the structure and properties of scaffold-free engineered auricular cartilage constructs. PLoS One 2014;9(8):e105170.
52. Ng KW, O'Conor CJ, Kugler LE, Cook JL, Ateshian GA, Hung CT. Transient supplementation of anabolic growth factors rapidly stimulates matrix synthesis in engineered cartilage. Ann Biomed Eng 2011 Oct;39(10):2491–2500.
53. Arévalo-Silva CA, Cao Y, Weng Y, Vacanti M, Rodríguez A, Vacanti CA, Eavey RD. The effect of fibroblast growth factor and transforming growth factor-beta on porcine chondrocytes and tissue-engineered autologous elastic cartilage. Tissue Eng 2001 Feb;7(1):81–88.
54. van Osch GJ, van der Veen SW, Buma P, Verwoerd-Verhoef HL. Effect of transforming growth factor-beta on proteoglycan synthesis by chondrocytes in relation to differentiation stage and the presence of pericellular matrix. Matrix Biol J Int Soc Matrix Biol 1998 Oct;17(6):413–424.
55. Blunk T, Sieminski AL, Gooch KJ, Courter DL, Hollander AP, Nahir AM, Langer R, Vunjak-Novakovic G, Freed LE. Differential effects of growth factors on tissue-engineered cartilage. Tissue Eng 2002 Feb;8(1):73–84.
56. van Osch GJ, van der Veen SW, Verwoerd-Verhoef HL. In vitro redifferentiation of culture-expanded rabbit and human auricular chondrocytes for cartilage reconstruction. Plast Reconstr Surg 2001 Feb;107(2):433–440.
57. Naumann A, Dennis JE, Aigner J, Coticchia J, Arnold J, Berghaus A, Kastenbauer ER, Caplan AI. Tissue engineering of autologous cartilage grafts in three-dimensional in vitro macroaggregate culture system. Tissue Eng 2004 Dec;10(11–12):1695–1706.
58. Liu Y, Zhang L, Zhou G, Li Q, Liu W, Yu Z, Luo X, Jiang T, Zhang W, Cao Y. In vitro engineering of human ear-shaped cartilage assisted with CAD/CAM technology. Biomaterials 2010 Mar;31(8):2176–2183.
59. Yanaga H, Imai K, Tanaka Y, Yanaga K. Two-stage transplantation of cell-engineered autologous auricular chondrocytes to regenerate Chondrofat composite tissue: clinical application in regenerative surgery. Plast Reconstr Surg 2013 Dec;132(6):1467–1477.
60. Pati F, Jang J, Ha D-H, Won Kim S, Rhie J-W, Shim J-H, Kim DH, Cho DW. Printing three-dimensional tissue analogues with decellularized extracellular matrix bioink. Nat Commun 2014 Jun 2;5:3935.
61. Beck EC, Barragan M, Libeer TB, Kieweg SL, Converse GL, Hopkins RA, Berkland CJ, Detamore MS. Chondroinduction from naturally derived cartilage matrix: a comparison between devitalized and Decellularized cartilage encapsulated in hydrogel pastes. Tissue Eng Part A 2016 Apr;22(7–8):665–679.
62. Visser J, Levett PA, te Moller NCR, Besems J, Boere KWM, van Rijen MHP, de Grauw JC, Dhert WJA, van Weeren PR, Malda J. Crosslinkable hydrogels derived from cartilage, meniscus, and tendon tissue. Tissue Eng Part A 2015 Apr;21(7–8):1195–1206.